Original article

Effects of gravity and buoyancy on spontaneous liquid-liquid imbibition in fractured porous media

Hui Cheng[1,2], Fuyong Wang[1,2]*

[1]*National Key Laboratory of Petroleum Resources and Engineering, China University of Petroleum, Beijing 102249, P. R. China*
[2]*Unconventional Petroleum Research Institute, China University of Petroleum, Beijing 102249, P. R. China*

Abstract:
Spontaneous imbibition in porous materials has received significant attention in recent decades; however, spontaneous liquid-liquid imbibition in fractures has not been well studied. Specifically, the mechanism behind the influence of gravity and buoyancy on the spontaneous imbibition of wetting phase fluid into fractured porous media remains uncertain. In this study, an analytical solution for spontaneous imbibition in fractured porous media under the influence of gravity and buoyancy is presented. The results show that imbibition velocity with buoyancy and gravity is faster than that without these forces. The effect of buoyancy and gravity on imbibition velocity increases with rising fracture aperture and length. When the fracture aperture is less than 1 μm, the relative deviation between imbibition height with and without gravity and buoyancy is about 50%. On the other hand, when the fracture aperture is greater than 1 μm, the relative deviation is proportional to the fracture aperture. The relative reduction in imbibition height over time is not obvious when the fracture aperture is the same. In the process of water-oil spontaneous imbibition, the effect of buoyancy and gravity is more pronounced at low oil-water interfacial tension. Therefore, the effect of buoyancy and gravity on spontaneous imbibition cannot be ignored under this condition.

1. Introduction

Spontaneous Imbibition (SI) is the process of a wetting phase fluid displacing a non-wetting phase fluid-saturated porous media driven by capillary force, which is a natural and widely occurring phenomenon with applications in engineering fields such as groundwater aquifers, petroleum reservoirs, and geotechnical engineering (Cai et al., 2012; Mehana et al., 2018; Andersen et al., 2019; Li et al., 2019b). In recent decades, many researchers have focused on SI in porous media, and these studies mainly addressed the SI process in the pores of matrix (Schmid and Geiger, 2012; Mason and Morrow, 2013; Shi et al., 2018; Tian et al., 2021). Recently, with the emergence of hydraulic fracturing in the development of unconventional petroleum and natural gas reservoirs such as shale reservoirs, researchers have begun to target SI processes

in fractured porous media (Cheng et al., 2015; Brabazon et al., 2019; Zhao et al., 2019, 2022). On the one hand, hydraulic fracturing creates numerous micro- and nanofractures in reservoirs (Mirzaei-Paiaman and Masihi, 2014; Liu et al., 2016; Zhou et al., 2023). On the other hand, natural fractures are commonly developed in unconventional oil and natural gas reservoirs (Wang and Cheng, 2020a; Liang et al., 2022; Tang et al., 2023; Zhang et al., 2023). Water-based fracturing fluids are the most frequently used fracturing fluids (Wang et al., 2019; Hossein Javadi and Fatemi, 2022; Zhao et al., 2022; Huang et al., 2023). Fracturing fluid can spontaneously imbibe into the reservoir during hydraulic fracturing operations, reducing the effective permeability of the reservoir and inhibiting the flow of crude oil (Hu et al., 2020; Zhao et al., 2022; Wang et al., 2023b; Zhang et al., 2023). Studying the mechanisms of spontaneous liquid-liquid imbibition in fractured porous

(a)   (b)   (c)
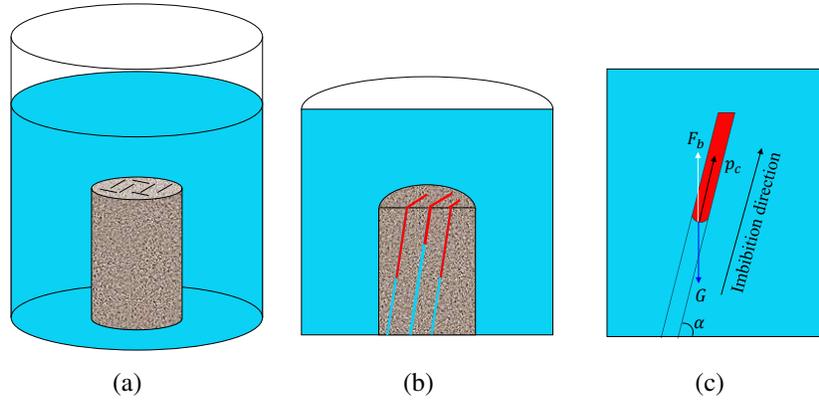
Fig. 1. Schematic diagram of SI of water-oil in fractured porous medium and concurrent SI in a single fracture (red represents oil (non-wetting phase) and blue represents water (wetting phase)).

media can help us understand the fluid flow process in fracture networks in shale oil reservoirs.

The SI behavior in fractured porous media is influenced by many factors, such as rock physics, fracture type and shape, fracture distribution, and heterogeneity (Cheng et al., 2015; Zhao et al., 2019; Hu et al., 2020; Liang et al., 2022). Due to the extremely low permeability in unconventional reservoirs, the fracture network serves as the primary seepage pathway for the flow of petroleum and natural gas from the reservoirs to the wellbore (Luo et al., 2018). More attention should be paid to spontaneous liquid-liquid imbibition in fractures (Zhang et al., 2017; Hu et al., 2020; Tokunaga, 2020; Zhao et al., 2022). Unconventional oil and gas reservoirs such as shale usually contain multiple types of fractures, such as tectonic and bedding fractures (Liang et al., 2022). Liu et al. (2017) found that bedding fracture is the most main type of fracture for shale oil reservoirs in the Junggar Basin. Liang et al. (2022) indicated that bedding fractures are widely developed for the shale oil formations in the Junggar Basin. Kong et al. (2021) studied the natural tectonic fracture characteristics in the Junggar Basin, and found that tectonic fractures can be divided into two main types: inclined fractures and bedding-parallel fractures. The above data provide evidence that research on fracture should intensify for the development of unconventional oil and gas resources.

The parallel plates model is one of the most classic physical models for describing fluid flow in fracture (Neuzil and Tracy, 1981; Moreno et al., 1985; Muralidhar, 1990). The cubic law derived based on Newton's law of viscosity and the parallel plates model is one of the most classical equations to calculate the flow rate of fracture. Schwiebert and Leong (1996) derived a model for describing the time-dependent SI height in a single fracture based on the model of the parallel plate, though the fluid gravity and the viscosity of the non-wetting phase were not taken into account. Wang and Cheng (2020b) also derived an equation for calculating the imbibition height in a single fracture. As opposed to the Schwiebert and Leong model, Wang and Cheng's model considers the effect of the gravity of the wetting phase fluid on the imbibition process, but the gravity and viscosity of

the non-wetting phase fluid are still not regarded (Wang and Cheng, 2020b).

For gas-saturated porous media, it is reasonable to ignore the gravity and viscosity of the non-wetting phase. This is because the viscosity and gravity of gas are generally negligible compared to liquids (Huang and Zhao, 2017; Wang et al., 2023a). However, in liquid-saturated porous media like shale oil reservoirs, the impact of the non-wetting phase on SI processes cannot be ignored, given the higher viscosity of oil compared to water (Hu et al., 2020; Tian et al., 2021, 2022; Zhao et al., 2022). Numerous studies have indicated the marked influence of fluid gravity on spontaneous imbibition (Cai et al., 2022; Salam and Wang, 2022; Wang and Yue, 2023). Based on Newton's law of viscosity, Cheng and Wang (2021) derived an analytical solution for spontaneous liquid-liquid imbibition with gravity and the viscosity of two-phase fluids. Recently, some researchers have noted that buoyancy may play a key role in the spontaneous imbibition of liquid-liquid systems under certain conditions. Wang and Zhao (2021) found that buoyancy has a significant effect on the SI behavior of water in tight oil reservoirs under low oil-water interfacial tension (IFT). In addition, a mathematical model was established by Wang and Zhao (2021) to study the effects of buoyancy on SI. However, there is no a clear conclusion on how much buoyancy affects SI in fractures.

The literature review reveals that SI in fracture has not been well studied; the mechanism of the effect of buoyancy and gravity on SI by wetting phase fluid into non-wetting phase fluid-saturated fractured porous media is still unclear. Therefore, this paper aims to i) develop a mathematical model for spontaneous liquid-liquid imbibition in fractured porous media with buoyancy and gravity; ii) establish a method to quantitatively evaluate the effects of buoyancy and gravity on SI; iii) conduct a sensitivity study to analyze the effect of buoyancy and gravity on SI in fractured porous media.

2. SI in a single fracture

Considering the effects of buoyancy and gravity, a new mathematical model for spontaneous liquid-liquid imbibition

in fractured porous media is developed. Figs. 1(a) and 1(b) present a schematic diagram of the SI of water-oil in the fractured porous media, and Fig. 1(c) depicts the concurrent SI in a single fracture. Water (displacing phase) is the wetting phase and oil (displaced phase) is the non-wetting phase. It is assumed that the fractured porous media consists of a bundle of plate fractures with different fracture apertures, and the SI is concurrent in the fracture; the fracture wall is impermeable, and the fluid exchange between the fracture and the matrix is ignored.

The parallel plates model is the most frequently used model to describe the fluid flow in fractures (Balankin et al., 2022; Trinchero et al., 2022; Chang et al., 2023; Li et al., 2023). According to the cubic law, the flow velocity v of the fluid in a single parallel plate fracture can be described as:

$$v = \frac{w^2 \Delta P}{12 \mu L} \tag{1}$$

where w denotes fracture aperture, μm; μ denotes fluid viscosity, mPa·s; L denotes fracture height, μm; ΔP denotes the pressure difference at both ends of the fracture, Pa. For the SI process of water into an oil-saturated fracture p_c, ΔP is composed of three pressures: capillary pressure, the gravity of fluids G, and buoyancy F_b. According to Young's equation, the capillary pressure can be expressed as (Washburn, 1921):

$$p_c = \frac{2\sigma \cos \theta}{w} \tag{2}$$

The gravity of liquids in a single fracture can be expressed as:

$$G = -[\rho_w x + \rho_o(L-x)] g \sin \alpha \tag{3}$$

For SI in a single fracture, buoyancy is caused by the hydraulic pressure difference between both ends of the fracture. The direction of buoyancy is opposite to the direction of gravity. Buoyancy in a single fracture can be calculated by:

$$F_b = \rho_w g L \sin \alpha \tag{4}$$

where σ denotes oil-water IFT, mN/m; θ denotes contact angle, °; ρ_w denotes water density, kg/m³; ρ_o denotes oil density, kg/m³; g denotes gravity acceleration, m/s²; α denotes the tilt angle of fracture, °; x denotes oil-water interface location, μm. Assuming that the fracture height of all fractures is the same as the core height, that is, $H = L \sin \alpha$, where H is the core height, μm.

By integrating Eqs. (2)-(4) into Eq. (1) , imbibition velocity in a single fracture can be expressed as:

$$v = \frac{2w\sigma \cos \theta + (\rho_w - \rho_o)(L-x)w^2 g \sin \alpha}{12[\mu_w x + \mu_o(L-x)]} \tag{5}$$

where u_w and μ_o denote water viscosity and oil viscosity respectively, mPa·s. Eq. (5) is the imbibition velocity expression in a single fracture when buoyancy and gravity are considered. Imbibition velocity can also be expressed as $v = dx/dt$. Then, Eq. (5) can be rewritten as:

$$\frac{dt}{dx} = \frac{12[\mu_w x + \mu_o(L-x)]}{2w\sigma \cos \theta + (\rho_w - \rho_o)(L-x)w^2 g \sin \alpha} \tag{6}$$

For convenience, the two constants in Eq. (6) are defined as follows: $\psi = -(\rho_w - \rho_o)w^2 g \sin \alpha$, $\zeta = 2w\sigma \cos \theta + (\rho_w - \rho_o)w^2 g L \sin \alpha$. Then, Eq. (6) can be rearranged as:

$$dt = \frac{12\mu_o L}{\psi x + \zeta} dx - \frac{12(\mu_o - \mu_w)x}{\psi x + \zeta} dx \tag{7}$$

By integrating Eq. (7), the solution of Eq. (7) can be obtained as:

$$t = \frac{12\mu_o L}{\psi} \ln(\psi x + \zeta) \\ - \frac{12\mu_o - \mu_w}{\psi^2} [\psi x + \zeta - \zeta \ln(\psi x + \zeta)] + C \tag{8}$$

where C is the integral constant. As $t = 0$ and $v = 0$, the constant C can be determined as:

$$C = \frac{12\mu_o - \mu_w}{\psi^2} (\zeta - \zeta \ln \zeta) - \frac{12\mu_o L}{\psi} \ln \zeta \tag{9}$$

By submitting Eq. (9) into Eq. (8), Eq. (8) can be expressed as:

$$t = \frac{12\mu_o L}{\psi} \ln \left(\frac{\psi}{\zeta} + 1 \right) \\ - \frac{12(\mu_o - \mu_w)}{\zeta^2} \left(\psi x + \zeta \ln \frac{\zeta}{\psi x + \zeta} \right) \tag{10}$$

Eq. (10) is the implicit analytical expression of Eq. (6). Eq. (10) can be used to calculate the imbibition time t for a given two-phase interface location x in a single fracture. However, it is difficult for Eq. (10) to calculate x in the given t because Eq. (6) has no explicit analytical solution. Here, a numerical method was developed to obtain the explicit expression of x, which allows researchers to predict it by entering the imbibition time. The numerical solution of Eq. (6) can be obtained using the finite difference method. For convenience, Eq. (6) can be written as:

$$12[\mu_w x + \mu_o(L-x)]dx \\ = [2w\sigma \cos \theta + (\rho_w - \rho_o)(L-x)w^2 g \sin \alpha]dt \tag{11}$$

First, the imbibition time and imbibition height are discretized. When the imbibition time increases from t_{j-1} to t_j, the imbibition height increases from x_{j-1} to x_j. Then, we integrate from x_{j-1} to x_j in the LHS of Eq. (11), and integrate from t_{j-1} to t_j in the RHS of Eq. (11). The imbibition height x in the RHS of Eq. (11) can be replaced by x_{j-1}.

$$\int_{x_{j-1}}^{x_j} 12[\mu_w x + \mu_o(L-x)]dx \\ = \int_{t_{j-1}}^{t_j} [2w\sigma \cos \theta + (\rho_w - \rho_o)(L-x_{j-1})gw^2 \sin \alpha]dt \tag{12}$$

Thus, one can obtain:

$$x_j^2 \left(\frac{1}{2}\mu_w - \frac{1}{2}\mu_o \right) + L\mu_o x_j = \frac{1}{2}\mu_w x_{j-1}^2 - \frac{1}{2}\mu_o x_{j-1}^2 \\ + \frac{w^2}{12} \left[\frac{2\sigma \cos \theta}{w} + (\rho_w - \rho_o)(L-x_{j-1})g \sin \alpha \right](t_j - t_{j-1}) \tag{13}$$

Then, the numerical solution of Eq. (6) can be obtained as follows:
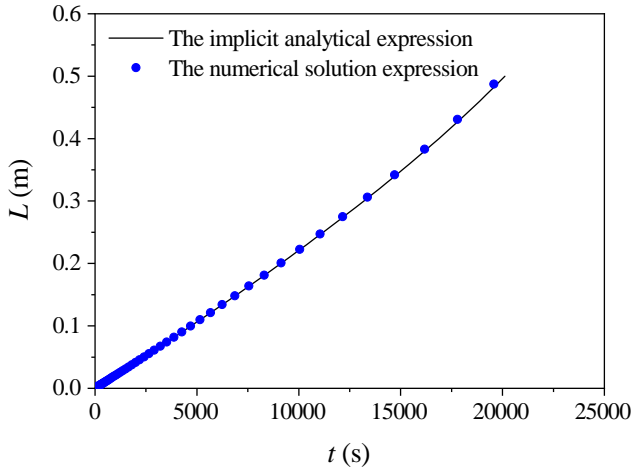
Fig. 2. Comparison of calculation results using Eqs. (10) and (14). The parameters of fracture and fluids used are $w = 10$ μm, $L = 0.5$ m, $\alpha = 90°$, $\sigma = 10$ mN/m, $\theta = 0°$, $\mu_o = 2.21$ mPa·s, $\mu_w = 1$ mPa·s, $\rho_o = 900$ kg/m^3, $\rho_w = 1,049.3$ kg/m^3, $g = 9.8$ m/s^2, $\alpha = 90°$.
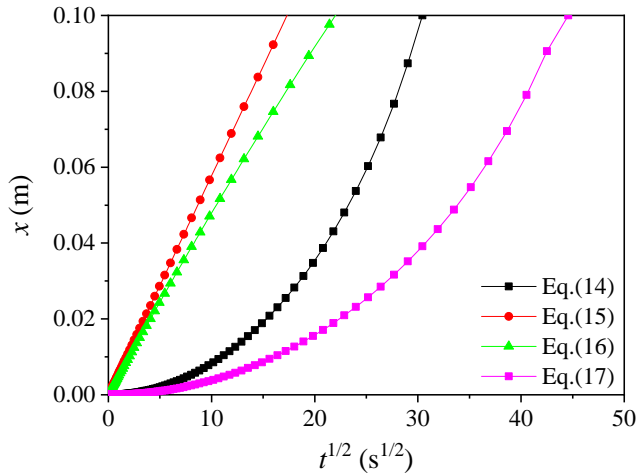
Fig. 3. Comparison of imbibition height versus $t^{\frac{1}{2}}$ calculated by Eqs. (14), (15), (16), and (17). The parameters of fracture and fluids used are $w = 10$ μm, $L = 0.1$ m, $\alpha = 90°$, $\sigma = 10$ mN/m, $\theta = 0°$, $\mu_o = 2.21$ mPa·s, $\mu_w = 1$ mPa·s, $\rho_o = 900$ kg/m^3, $\rho_w = 1,049.3$ kg/m^3, $g = 9.8$ m/s^2, $\alpha = 90°$.

$$
\begin{cases}
x_j = \dfrac{L\mu_o - \sqrt{(L\mu_o)^2 - 2(\mu_o - \mu_w)\Gamma}}{\mu_o - \mu_w} \\[2mm]
\Gamma = \mu_o x_{j-1} - \dfrac{1}{2}(\mu_o - \mu_w)x_{j-1}^2 + \dfrac{w^2}{12} \\[2mm]
\left[\dfrac{2\sigma\cos\theta}{w} + (\rho_w - \rho_o)(L - x_{j-1})g\sin\alpha\right](t_j - t_{j-1})
\end{cases}
\tag{14}
$$

It should be noted that the proposed model is a one-dimensional model as it is derived based on the assumption of concurrent SI. The results calculated using Eqs. (10) and (14) are compared (Fig. 2) under the same parameters of fracture and fluids. The curves of imbibition height versus imbibition time using Eqs. (10) and (14) aalmost overlap, indicating that the numerical solution method is reliable.
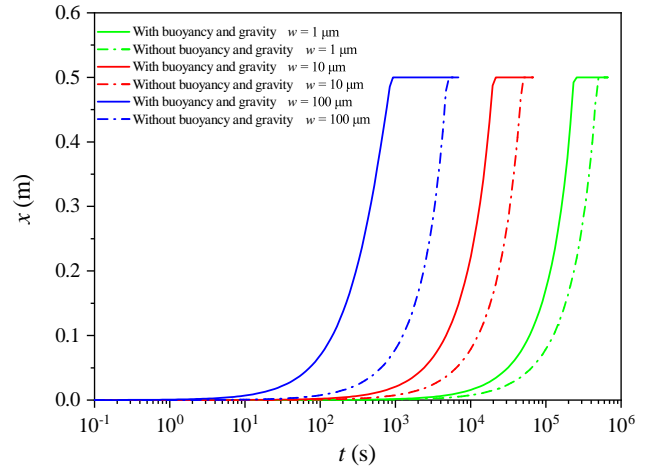
Fig. 4. Effect of displaced phase buoyancy on SI in fractures with aperture $w = 1$ μm, $w = 10$ μm and $w = 100$ μm (other parameters are $\sigma = 10$ mN/m, $\theta = 0°$, $\mu_o = 2.21$ mPa·s, $\mu_w = 1$ mPa·s, $\rho_w = 1,049.3$ kg/m^3, $\rho_o = 900$ kg/m^3, $L = 0.5$ m, $g = 9.8$ m/s^2, $\alpha = 90°$).

For SI in a horizontal oil-saturated fracture, which means that the SI process is only driven by capillary pressure, the imbibition location can be calculated as (Cheng and Wang, 2021):

$$
x = \frac{\mu_o L - \sqrt{(\mu_o L)^2 - (\mu_o - \mu_w)\frac{w\sigma\cos\theta}{6}t}}{\mu_o - \mu_w}
\tag{15}
$$

Eq. (15) is derived by Cheng and Wang (2021). Schwiebert and Leong (1996) derived an equation for describing SI only driven by capillary pressure in a single parallel fracture:

$$
x = \sqrt{\frac{w\sigma\cos\theta}{3\mu}t}
\tag{16}
$$

This model is a classical model, but it ignores the effect of gravity of the fluids and the viscosity of the displaced phase on SI. Wang and Cheng (2020b) also derived an equation for describing SI in a single fracture:

$$
x = \frac{A}{B}\left[1 + W\left(-e^{-1 - \frac{B^2}{A}t}\right)\right]
\tag{17}
$$

where $A = w\sigma\cos\theta/(6\mu_w)$ and $B = w^2\rho_w g/(12\mu_w)$. However, the influence of the viscosity of the displaced phase on SI is not considered in this model. Unlike Eq. (16), Eq. (17) considers the effect of gravity on SI.

The imbibition height versus $t^{1/2}$ calculated by different models were compared (Fig. 3). The imbibition rate calculated by Eqs. (16) and (17) is significantly faster than the imbibition rate calculated by the other two models. The reason is that Eqs. (16) and (17) ignore the effect of viscosity of the displaced phase on SI. When the effect of buoyancy on SI is considered, the imbibition rate calculated by Eq. (14) is significantly faster than the imbibition rate calculated by the Eq. (15).

The imbibition velocity with buoyancy and gravity calculated by Eq. (14) is slightly faster than that without buoyancy and gravity calculated by Eq. (15) (Fig. 4). As the fracture aperture increases from 1 to 10 μm and then to 100 μm, the difference between the curves of imbibition height with and
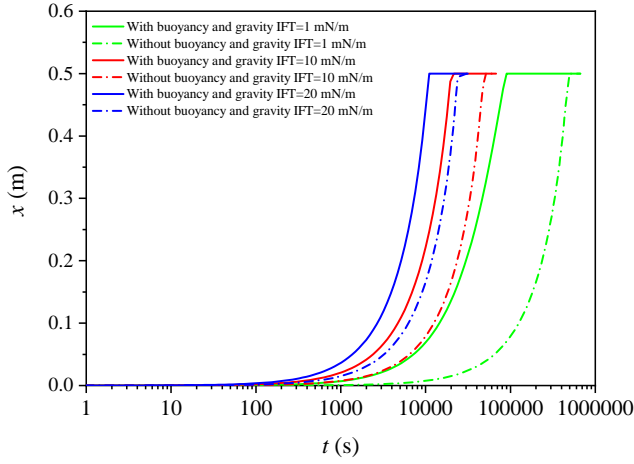
Fig. 5. Effect of oil-water IFT on SI in fracture with aperture $w = 10$ μm (other parameters are: $\theta = 0°$, $\mu_o = 2.21$ mPa·s, $\mu_w = 1$ mPa·s, $\rho_w = 1,049.3$ kg/m^3, $\rho_o = 900$ kg/m^3, $L = 0.5$ m, $g = 9.8$ m/s^2, $\alpha = 90°$).
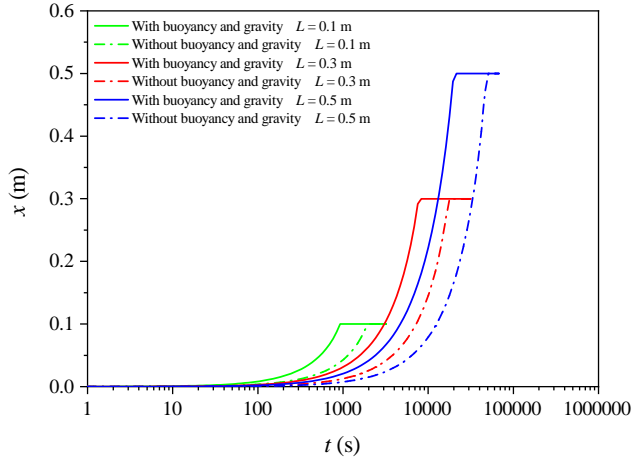
Fig. 6. Effect of fracture length on SI in fracture with aperture $w = 10$ μm (other parameters are: $\sigma = 10$ mN/m, $\theta = 0°$, $\mu_o = 2.21$ mPa·s, $\mu_w = 1$ mPa·s, $\rho_w = 1,049.3$ kg/m^3, $\rho_o = 900$ kg/m^3, $g = 9.8$ m/s^2, $\alpha = 90°$).

without buoyancy and gravity versus imbibition time becomes significant, as SI is driven by the buoyancy and capillary pressure for Eq. (14) , but the capillary pressure is the only driving pressure in the SI process for Eq. (15). As the fracture aperture increases, the volume of the crude oil in the fracture becomes larger, and the buoyancy and gravity become significant.

When the oil-water IFT decreases from 20 to 10 mN/m and then to 1 mN/m, the imbibition velocity with and without buoyancy and gravity decreases, but the difference between the curves of imbibition height with and without buoyancy and gravity versus imbibition time increases when the oil-water interfacial tension is the same (Fig. 5).

When the fracture length decreases from 0.5 to 0.3 m and then to 0.1 m, the imbibition velocity with and without buoyancy and gravity increases, but the difference between the
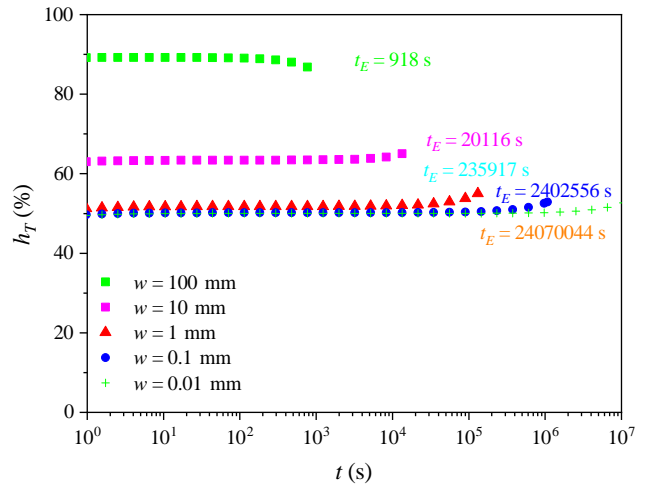
Fig. 7. The value of η_T varying with imbibition time in fractures with different apertures (other parameters are: $\sigma = 10$ mN/m, $\theta = 0°$, $\mu_o = 2.21$ mPa·s; $\mu_w = 1$ mPa·s, $\rho_w = 1,049.3$ kg/m^3, $\rho_o = 900$ kg/m^3, $L = 0.5$ m, $g = 9.8$ m/s^2, $\alpha = 90°$).

curves of imbibition height with and without buoyancy and gravity versus imbibition time are almost the same when the SI process ends (Fig. 6).

When the two-phase interface reaches the end of the fracture, the SI process comes to an end. The end time t_E of SI with buoyancy and gravity can be obtained by using L to replace x in Eq. (10):

$$t_E = \frac{12\mu_o L}{\psi} \ln\left(\frac{\psi}{\zeta}L + 1\right)$$
$$- \frac{12(\mu_o - \mu_w)}{\psi^2}\left(\psi L + \zeta \ln\frac{\zeta}{\psi L + \zeta}\right) \tag{18}$$

The relative reduction in imbibition height η_T varying with imbibition time is defined for evaluating the influence of buoyancy and gravity on SI as follows:

$$\eta_T = \frac{L(t) - L_w(t)}{L(t)} \times 100\%, \quad t \le t_E \tag{19}$$

where $L(t)$ represents imbibition height without buoyancy and gravity, μm; $L_w(t)$ denotes imbibition height with buoyancy and gravity, μm. Changes in the value of η_T over the imbibition time are not apparent under the same fracture apertures (Fig. 7). Taking the fracture with aperture $w = 0.01$ μm as an example, the value of η_T increases from 49.82% to 50.03% with the increase in imbibition time from 1 to 10^6 s. Whether $w = 0.01$ or 100 μm, the change in the value of η_T with increasing imbibition time is less than 5%. When $w \le 1$ μm, the value of η_T is about 50%; when $w > 1$ μm, η_T increases with an increasing fracture aperture. This means that the effects of buoyancy and gravity on SI are not negligible, even in small fractures with a fracture aperture of less than 1 μm.

Another parameter η_L is defined to further evaluate the influence of buoyancy and gravity on SI as follows:

$$\eta_L = \frac{L - L_w(t_E)}{L} \times 100\% \tag{20}$$
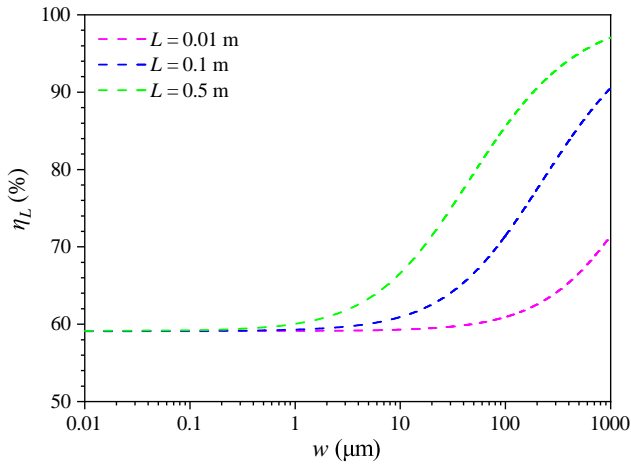
Fig. 8. Curves of η_L versus fracture aperture in fractures with different fracture lengths in a semi-log plot (other parameters are: $\sigma = 10$ mN/m, $\theta = 0°$, $\mu_o = 2.21$ mPa·s, $\mu_w = 1$ mPa·s, $\rho_w = 1{,}049.3$ kg/m^3, $\rho_o = 900$ kg/m^3, $g = 9.8$ m/s^2, $\alpha = 90°$).
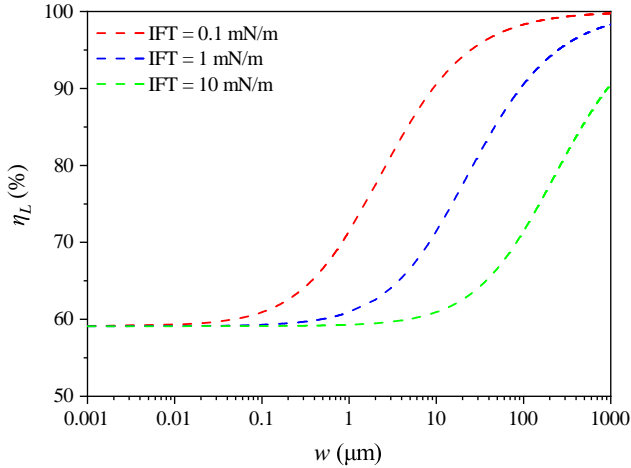
Fig. 9. Curves of η_L versus fracture aperture at different oil-water IFT in a semi-log plot (other parameters are: $L = 0.1$ m, $\theta = 0°$, $\mu_o = 2.21$ mPa·s, $\mu_w = 1$ mPa·s, $\rho_w = 1{,}049.3$ kg/m^3, $\rho_o = 900$ kg/m^3, $g = 9.8$ m/s^2, $\alpha = 90°$).

where $L_w(t_E)$ represents the location of the two-phase interface by using the end time of SI with buoyancy and gravity calculated by Eq. (18), s. Since the imbibition velocity calculated by Eq. (14) (with buoyancy and gravity) is faster than that calculated by Eq. (15) (without buoyancy and gravity), when the location of the two-phase interface x calculated by Eq. (14) reaches the fracture length L, then x calculated by Eq. (15) is still less than the fracture length L. Therefore, η_L means the relative reduction in imbibition height with and without buoyancy and gravity. The larger η_L is, the larger the effect of buoyancy on SI.

Taking a fracture with length $L = 0.1$ m as an example, when the fracture aperture is smaller than 1 μm, the value of η_L slowly increases with the fracture aperture in a semi-log plot (Fig. 8). When w is greater than 1 μm, η_L first increases rapidly with the fracture aperture increase, then increases slow-
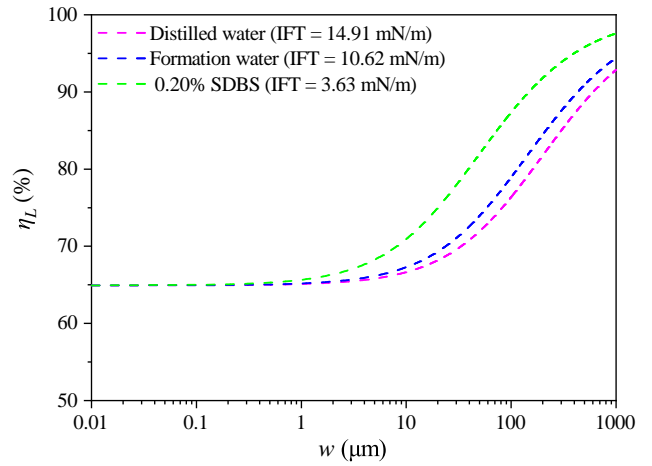
Fig. 10. Curves of η_L versus fracture aperture for distilled water, formation water and 0.20% SDBS (dodecylbenzene sulfonate solution) in a semi-log plot (other parameters are: $L = 0.05$ m, $\theta = 55°$, $\mu_o = 4.8$ mPa·s, $\mu_w = 1$ mPa·s, $\rho_w = 1{,}049.3$ kg/m^3, $\rho_o = 798$ kg/m^3, $g = 9.8$ m/s^2, $\alpha = 90°$. Data from Yang et al. (2022)).

ly in a semi-log plot. The effects of buoyancy and gravity on SI strengthen with increasing w and L. The value of η_L increases from 59.11% to 90.55% with w rising from 0.01 to 1,000 μm when $L = 0.1$ m. The value of η_L increases from 60.93% to 85.58% with L increasing from 0.01 to 0.5 m for $w = 100$ μm.

Taking IFT = 0.1 mN/m as an example, as w increases from 0.1 to 1,000 μm, η_L slowly increases when $w \leq 0.1$ μm, then sharply increases with w increasing from 0.1 to 100 μm, and finally slowly increases when $w > 100$ μm in a semi-log plot (Fig. 9). The value of η_L sharply increases from 59.11% to 98.31% with w increasing from 0.001 to 1,000 μm at an oil-water IFT equal to 1 mN/m. The value of η_L sharply increases from 60.93% to 90.54% with ITF decreasing from 10 to 0.1 mN/m when $w = 10$ μm. This means that the effects of buoyancy and gravity on SI are more pronounced under low interfacial tension conditions.

Buoyancy and gravity have a significant effect on SI in both small and large fractures (Fig. 10). For distilled water, the value of η_L increases from 64.92% to 92.86% with w increasing from 0.01 to 1,000 μm. For formation water, the value of η_L increases from 64.92% to 94.41% with w increasing from 0.01 to 1,000 μm. For 0.20% SDBS, the value of η_L increases from 64.93% to 97.59% with w increasing from 0.01 to 1,000 μm. Compared with distilled water and formation water, buoyancy and gravity have a more pronounced effect on the imbibition of spontaneous surfactant solutions into oil-saturated fractures. The reason is that surfactants reduce the oil-water IFT but have little effect on gravity and buoyancy, which will lead to a more pronounced effect of these two parameters on SI. The effect of buoyancy and gravity on SI is not negligible under low oil-water IFT conditions.

The Bond number N_b is a dimensionless parameter used in evaluating the effects of gravitational forces and interfacial tension forces on SI (Schechter et al., 1994; Meng et al., 2016;

Chang et al., 2022; Qi et al., 2022). A larger N_b means that gravitational forces have a greater effect on SI (Schechter et al., 1994). The expression of N_b for water imbibition into oil-saturated porous media can be given as:

$$N_b = \frac{\Delta \rho g w^2}{\sigma} \tag{21}$$

where $\Delta \rho$ denotes the density difference between oil and water, kg/m^3.

For fracture aperture $w = 1$ μm, the value of N_b decreases from 1.46×10^{-4} to 4.88×10^{-8} as the oil-water IFT increases from 0.01 to 30 mN/m (Fig. 11). For $w = 10$ μm, the value of N_b decreases from 1.46×10^{-2} to 4.88×10^{-6} as the oil-water IFT increases from 0.01 to 30 mN/m; for $w = 100$ μm, the value of N_b decreases from 1.46 to 4.88×10^{-4} as the oil-water IFT increases from 0.01 to 30 mN/m. As w increases, the curves of η_L versus N_b move to the right in the semi-log plot, which indicates that gravitational forces start to dominate in SI.

3. SI in fractured porous media

3.1 Mathematical model

Some studies have established that the distribution of fracture aperture can be characterized on a logarithmic scale by the Gaussian probability density function (PDF) (Neuzil and Tracy, 1981; Moreno et al., 1985; Li et al., 2019a). Therefore, in this paper, the Gaussian PDF on the logarithmic scale is used to describe the distribution of fracture aperture on the core scale. The Gaussian PDF $f(w)$ is expressed as (Cao et al., 2019):

$$f(w) = \frac{1}{\sqrt{2\pi} \log \delta} e^{-\frac{\log w - \log \beta}{2(\log \delta)^2}} \tag{22}$$

where $\log \beta$ represents the mean value of the logarithmic fracture aperture, μm; $\log \delta$ denotes the standard deviation of the logarithmic fracture aperture, μm. According to Cheng and Wang (2021), the total number of fractures N can be calculated by:

$$N = \frac{\phi \pi d^2 \sin \alpha}{4\gamma \int_{w_{\min}}^{w_{\max}} f(w)w^2 \mathrm{d}w} \tag{23}$$

where γ denotes the ratio of fracture width L_w to fracture aperture w, dimensionless; d denotes core diameter, cm; ϕ denotes porosity, %. Fig. 12 is a schematic diagram of the fractured porous media.

The number of fractures with a particular aperture w can be stated by the incremental number $n(w)$:

$$n(w) = Nf(w) \tag{24}$$

The total oil production $Q(t)$ of the core can be calculated by:

$$Q(t) = \gamma N \int_{w_{\min}}^{w_{\max}} w^2 x f(w) \mathrm{d}w \tag{25}$$

Then, the oil recovery factor $R(t)$ can be calculated by:

$$R(t) = \frac{4Q(t)}{\pi d^2 L \phi} \tag{26}$$
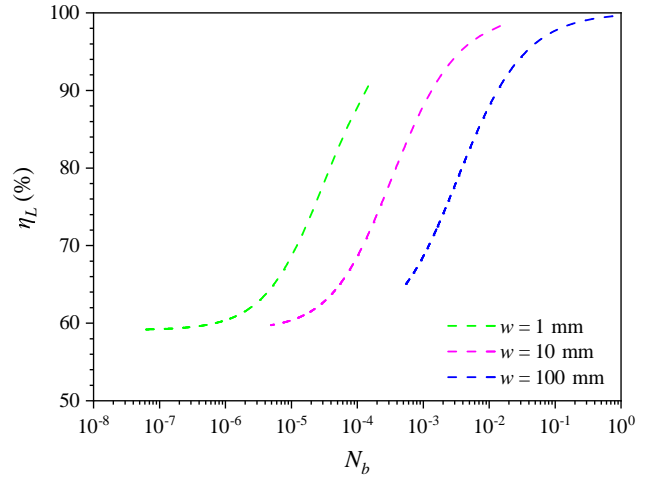
Fig. 11. The value of η_T varies with the Bond number in fractures with different apertures (other parameters are: $\theta = 0°$, $\mu_o = 2.21$ mPa·s, $\mu_w = 1$ mPa·s, $\rho_w = 1,049.3$ kg/m^3, $\rho_o = 900$ kg/m^3, $L = 0.1$ m, $g = 9.8$ m/s^2, $\alpha = 90°$).
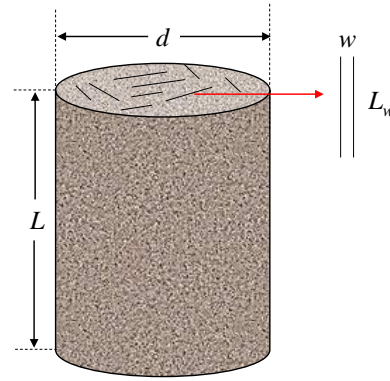
Fig. 12. Schematic diagram of fractured porous media (where w denotes fracture aperture, L_w denotes fracture width, d denotes core diameter, and L denotes fracture height, which is equal to the core height).

3.2 Sensitivity analysis

In this section, the effects of gravity and buoyancy on the SI in fractured porous media are analyzed using the Gaussian distribution of fracture apertures as an analytical basis. The parameters of fracture and fluids used for sensitivity analysis are listed in Table 1.

The smaller the standard deviation of logarithmic fracture aperture, the more concentrated the distribution of fracture aperture (Fig. 13(a)). When the fracture apertures follow Gaussian distribution, the imbibition rate increases with the standard deviation of the logarithmic fracture aperture increase (Fig. 13(b)). When buoyancy and gravity are considered, the fractured porous media have a faster imbibition rate. For Gaussian distribution, the number of fractures at mean value β is the largest (Fig. 14(a)). The imbibition rate increases with the rising mean value when the fracture apertures follow Gaussian distribution (Fig. 14(b)).
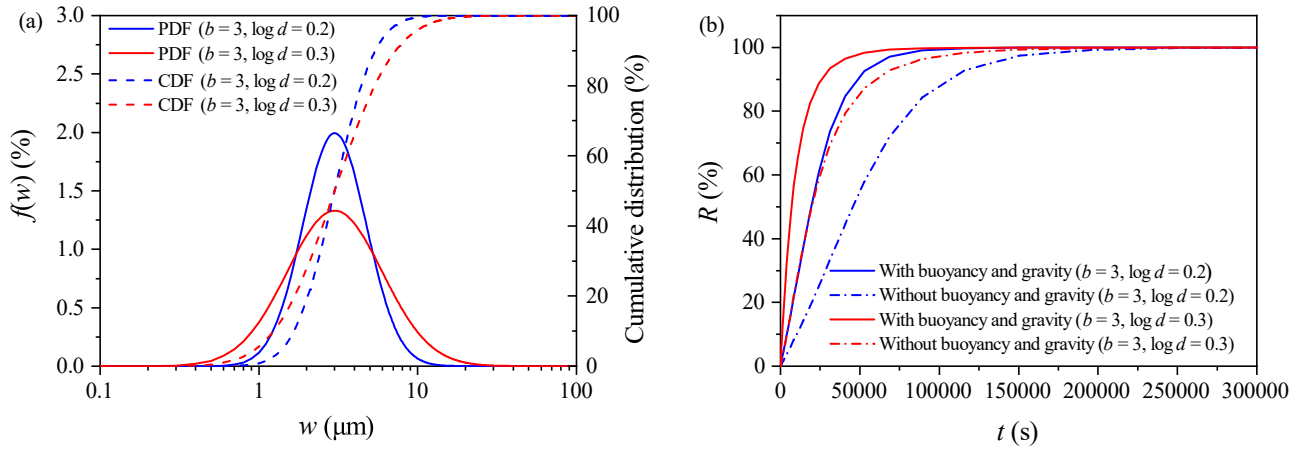
Fig. 13. (a) Gaussian PDF and cumulative distribution function (CDF) of fracture aperture distribution with $\log \delta = 0.2$ and 0.3; (b) the corresponding curves of oil recovery factor by SI with and without buoyancy versus imbibition time.

Table 1. Parameters of fracture and fluids used for sensitivity analysis.

Parameters	Value
Porosity (%)	20
Fracture height (m)	0.1
Core diameter (cm)	2.0
Minimum fracture aperture (μm)	0.1
Maximum fracture aperture (μm)	100
Ratio of fracture width to fracture aperture	20
Tilt angle of fracture (degree)	90
Water viscosity (mPa·s)	1
Oil viscosity (mPa·s)	2.21
Oil-water IFT (mN/m)	10
Water density (kg/m^3)	1,049.3
Oil density, (kg/m^3)	900
Contact angle (degree)	0
Gravity acceleration (m/s^2)	9.8

The difference between the imbibition rate without buoyancy and gravity is significantly greater than that with buoyancy and gravity at IFT = 10 mN/m and IFT = 1 mN/m (Fig. 15). This means that oil-water IFT has a more pronounced effect on SI without buoyancy and gravity when the fracture apertures follow Gaussian distribution. When the oil-water IFT is equal to 10 mN/m, the curves of oil recovery factor by SI with and without buoyancy and gravity versus imbibition time are close, indicating that the effect of buoyancy and gravity on the imbibition rate is negligible at high oil-water IFT. The imbibition rate with buoyancy and gravity is significantly faster than the imbibition rate without buoyancy and gravity at IFT = 1 mN/m, which means that the effect of buoyancy and gravity on SI cannot be ignored under low oil-water IFT conditions.

4. Conclusions

Based on the results of this study, the following conclusions can be obtained:

1) The imbibition rate with buoyancy and gravity is higher than that without buoyancy and gravity. The effect of buoyancy and gravity on imbibition velocity increases with rising fracture aperture and length, and this effect is stronger with decreasing oil-water IFT.

2) Two dimensionless parameters η_T and η_L are defined to quantitatively evaluate the effect of buoyancy and gravity on SI in a single fracture. When the fracture aperture $w \leq 1$ μm, the value of η_T is about 50%; when $w > 1$ μm, the value of η_T increases with increasing fracture aperture. The changes in the value of η_T over the imbibition time are not obvious when w is the same. As the value of w increases from 0.01 to 1,000 μm, η_L first increases slowly, then sharply, and finally slowly in a semi-log plot. The value of η_L increases with the increasing fracture aperture and length. The value of η_L decreases with the increasing oil-water IFT. In the SI process of water-oil, the effect of buoyancy and gravity is more pronounced when the oil-water IFT is lower.

3) When the fracture apertures follow Gaussian distribution, the imbibition rate increases with the standard deviation of the logarithmic fracture aperture, and the mean value increases. The effect of buoyancy and gravity on SI cannot be ignored under low oil-water IFT conditions when the fracture apertures follow Gaussian distribution.

Conflict of interest

The authors declare no competing interest.
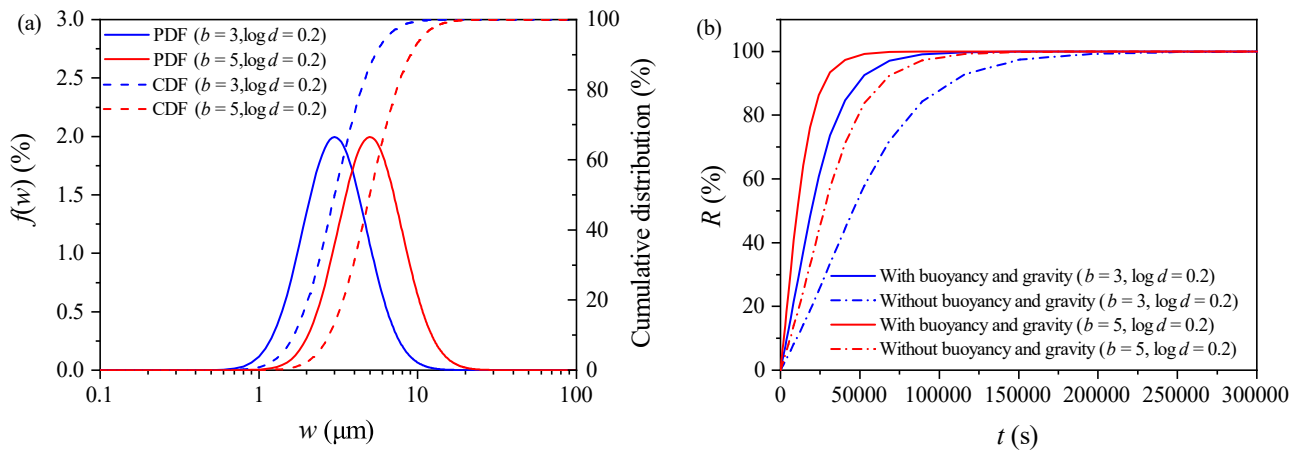
Fig. 14. (a) Gaussian PDF and CDF of fracture aperture distribution with $\beta = 3$ and 5; (b) the corresponding curves of oil recovery factor by SI with and without buoyancy versus imbibition time.
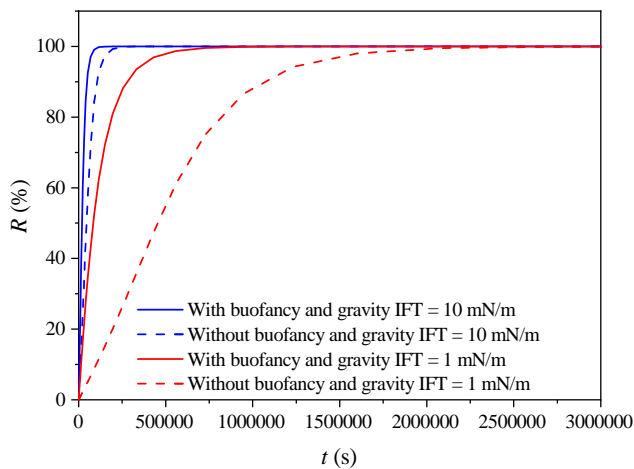
Fig. 15. Curves of oil recovery factor by SI with and without buoyancy versus imbibition time under different oil-water IFT values (other parameters are $\beta = 3$ and $\log \delta = 0.2$).

References

Andersen, P. Ø., Qiao, Y., Standnes, D. C., et al. Cocurrent spontaneous imbibition in porous media with the dynamics of viscous coupling and capillary backpressure. SPE Journal, 2019, 24(1): 158-177.

Balankin, A. S., Ramírez-Joachin, J., González-López, G., et al. Formation factors for a class of deterministic models of pre-fractal pore-fracture networks. Chaos, Solitons & Fractals, 2022, 162: 112452.

Brabazon, J. W., Perfect, E., Gates, C. H., et al. Spontaneous imbibition of a wetting fluid into a fracture with opposing fractal surfaces: Theory and experimental validation. Fractals, 2019, 27(1): 1940001.

Cai, J., Chen, Y., Liu, Y., et al. Capillary imbibition and flow of wetting liquid in irregular capillaries: A 100-year review. Advances in Colloid and Interface Science, 2022, 304: 102654.

Cai, J., Hu, X., Standnes, D. C., et al. An analytical model for spontaneous imbibition in fractal porous media including gravity. Colloids and Surfaces A: Physicochemical and Engineering Aspects, 2012, 414: 228-233.

Cao, R., Xu, Z., Cheng, L., et al. Study of single phase mass transfer between matrix and fracture in tight oil reservoirs. Geofluids, 2019, 2019: 1038412.

Chang, B., Cao, C., Zhang, Y., et al. Discrete fracture model with unsteady-state adsorption and water-gas flow for shale-gas reservoirs. Energy Reports, 2023, 9: 371-386.

Chang, Y., Yao, Y., Liu, D., et al. Behavior and mechanism of water imbibition and its influence on gas permeability during hydro-fracturing of a coalbed methane reservoir. Journal of Petroleum Science and Engineering, 2022, 208: 109745.

Cheng, C. L., Perfect, E., Donnelly, B., et al. Rapid imbibition of water in fractures within unsaturated sedimentary rock. Advances in Water Resources, 2015, 77: 82-89.

Cheng, H., Wang, F. Mathematical model of the spontaneous imbibition of water into oil-saturated fractured porous media with gravity. Chemical Engineering Science, 2021, 231: 116317.

Hossein Javadi, A., Fatemi, M. Impact of salinity on fluid/fluid and rock/fluid interactions in enhanced oil recovery by hybrid low salinity water and surfactant flooding from fractured porous media. Fuel, 2022, 329: 125426.

Hu, Y., Zhao, C., Zhao, J., et al. Mechanisms of fracturing fluid spontaneous imbibition behavior in shale reservoir: A review. Journal of Natural Gas Science and Engineering, 2020, 82: 103498.

Huang, X., Liu, F., Zhang, P., et al. Application of microgel latex in water-based drilling fluid to stabilize the fractured formation. Geoenergy Science and Engineering, 2023, 228: 212016.

Huang, X., Zhao, Y. Characterization of pore structure, gas

adsorption, and spontaneous imbibition in shale gas reservoirs. Journal of Petroleum Science and Engineering, 2017, 159: 197-204.

Kong, X., Zeng, J., Tan, X., et al. Natural tectonic fractures and their formation stages in tight reservoirs of Permian Lucaogou Formation, Jimsar Sag, southern Junggar Basin, NW China. Marine and Petroleum Geology, 2021, 133: 105269.

Li, Y., Chen, X., Shao, Y. 3D natural fracture model of shale reservoir based on petrophysical characterization. Journal of Structural Geology, 2023, 166: 104763.

Li, X., Jiang, Z., Couples, G. G. A Stochastic method for modelling the geometry of a single fracture: spatially controlled distributions of aperture, roughness and anisotropy. Transport in Porous Media, 2019a, 128(2): 797-819.

Li, C., Singh, H., Cai, J. Spontaneous imbibition in shale: A review of recent advances. Capillarity, 2019b, 2(2): 17-32.

Liang, C., Liu, A., Luo, Q., et al. Differences in imbibition efficiency between bedding and tectonic fractures in the lucaogou formation in the Jimusar sag: Evidence from simulation experiments. Frontiers in Earth Science, 2022, 10: 918244.

Liu, D., Chen, Z., Luo, Q., et al. Development characteristics and controlling factors of natural fractures in Permian Lucaogou Formation tight reservoir in Jimsar sag, Junggar Basin. China Petroleum Exploration, 2017, 4(22): 36-47. (in Chinese)

Liu, R., Yu, L., Jiang, Y. Fractal analysis of directional permeability of gas shale fracture networks: A numerical study. Journal of Natural Gas Science and Engineering, 2016, 33: 1330-1341.

Luo, W., Tang, C., Zhou, Y., et al. A new semi-analytical method for calculating well productivity near discrete fractures. Journal of Natural Gas Science and Engineering. 2018, 57: 216-223.

Mason, G., Morrow, N. R. Developments in spontaneous imbibition and possibilities for future work. Journal of Petroleum Science and Engineering, 2013, 110: 268-293.

Mehana, M., Al Salman, M., Fahes, M. Impact of salinity and mineralogy on slick water spontaneous imbibition and formation strength in shale. Energy & Fuels, 2018, 32(5): 5725-5735.

Meng, Q., Liu, H., Wang, J., et al. Effect of gravity on spontaneous imbibition from cores with two ends open in the frontal flow period. Journal of Petroleum Science and Engineering, 2016, 141: 16-23.

Mirzaei-Paiaman, A., Masihi, M. Scaling of recovery by cocurrent spontaneous imbibition in fractured petroleum reservoirs. Energy Technology, 2014, 2(2): 166-175.

Moreno, L., Neretnieks, I., Eriksen, T. Analysis of some laboratory tracer runs in natural fissures. Water Resources Research, 1985, 21(7): 951-958.

Muralidhar, K. Flow and transport in single rock fractures. Journal of Fluid Mechanics, 1990, 215(1): 481.

Neuzil, C. E., Tracy, J. V. Flow through fractures. Water Resources Research, 1981, 17(1): 191-199.

Qi, Z., Han, M., Chen, S., et al. Surfactant enhanced imbibition in carbonate reservoirs: Effect of IFT reduction and surfactant partitioning. JCIS Open, 2022, 5: 100045.

Salam, A., Wang, X. An analytical solution on spontaneous imbibition coupled with fractal roughness, slippage and gravity effects in low permeability reservoir. Journal of Petroleum Science and Engineering, 2022, 208: 109501.

Schechter, D. S., Zhou, D., Orr, F. M. Low IFT drainage and imbibition. Journal of Petroleum Science and Engineering, 1994, 11(4): 283-300.

Schmid, K. S., Geiger, S. Universal scaling of spontaneous imbibition for water-wet systems. Water Resources Research, 2012, 101: 44-61.

Schwiebert, M., Leong, K. Underfill flow as viscous flow between parallel plates driven by capillary action. IEEE Transactions on Components, Packaging, and Manufacturing Technology: Part C, 1996, 2(19): 133-137.

Shi, Y., Yassin, M. R., Dehghanpour, H. A modified model for spontaneous imbibition of wetting phase into fractal porous media. Colloids and Surfaces A: Physicochemical and Engineering Aspects, 2018, 543: 64-75.

Tang, X., Zhu, H., Che, M., et al. Complex fracture propagation model and plugging timing optimization for temporary plugging fracturing in naturally fractured shale. Petroleum Exploration and Development, 2023, 50(1): 152-165.

Tian, W., Wu, K., Chen, Z., et al. A relative permeability model considering nanoconfinement and dynamic contact angle effects for tight reservoirs. Energy, 2022, 258: 124846.

Tian, W., Wu, K., Gao, Y., et al. A critical review of enhanced oil recovery by imbibition: Theory and practice. Energy & Fuels, 2021, 35(7): 5643-5670.

Tokunaga, T. K. Simplified green-ampt model, imbibition-based estimates of permeability, and implications for leak-off in hydraulic fracturing. Water Resources Research, 2020, 56: e2019WR026919.

Trinchero, P., Sanglas, J., Iraola, A., et al. On the parameterisation of dual-continuum models for reactive transport modelling in fractured media. Journal of Hydrology, 2022, 615: 128691.

Wang, F., Cheng, H. A fractal permeability model for 2D complex tortuous fractured porous media. Journal of petroleum science and engineering, 2020a, 188: 106938.

Wang, F., Cheng, H. Effect of gravity on spontaneous imbibition of the wetting phase into gas-saturated tortuous fractured porous media: Analytical solution and diagnostic plot. Advances in Water Resources, 2020b, 142: 103657.

Wang, G., Huang, T., Yan, S. Experimental study of the fracturing-wetting effect of VES fracturing fluid for the coal seam water injection. Journal of Molecular Liquids, 2019, 295: 111715.

Wang, W., Xie, Q., Li, J., et al. Fracturing fluid imbibition impact on gas-water two phase flow in shale fracture-matrix system. Natural Gas Industry B, 2023a, 10(4): 323-332.

Wang, C., Yang, Y., Nie, X., et al. Effect of Micro pore-throat on porosity and permeability of dual media digital rock.

Chinese Journal of Computational Physics, 2023b, 40(5): 606-613. (in Chinese)

Wang, F., Yue, H. A comprehensive mathematical model for spontaneous imbibition in oil-saturated fractured tight sandstones: Incorporating fracture distribution, displacement pressure, gravity, and buoyancy effects. Physics of Fluids, 2023, 35(6): 062122.

Wang, F., Zhao, J. Mathematical modeling of gravity and buoyancy effect on low interfacial tension spontaneous imbibition in tight oil reservoirs. AIChE Journal, 2021, 67(9): e17332.

Washburn, E. W. The dynamics of capillary flow. Physical Review, 1921, 3(17): 273-283.

Yang, K., Wang, F., Zhao, J. Experimental study of surfactant-enhanced spontaneous imbibition in fractured tight sandstone reservoirs: The effect of fracture distribution. Petroleum Science, 2022, 20(1): 370-381.

Zhang, X., Ye, Q., Deng, J., et al. Experimental study and mechanism analysis of spontaneous imbibition of surfactants in tight oil sandstone. Capillarity, 2023, 7(1): 1-12.

Zhang, C., Zhu, D., Luo, Q., et al. Major factors controlling fracture development in the Middle Permian Lucaogou Formation tight oil reservoir, Junggar Basin, NW China. Journal of Asian Earth Sciences, 2017, 146: 279-295.

Zhao, M., Liu, S., Gao, Z., et al. The spontaneous imbibition mechanisms for enhanced oil recovery by gel breaking fluid of clean fracturing fluid. Colloids and Surfaces A: Physicochemical and Engineering Aspects, 2022, 650: 129568.

Zhao, Y., Wu, Y., Han, S., et al. Water sorptivity of unsaturated fractured sandstone: Fractal modeling and neutron radiography experiment. Advances in Water Resources, 2019, 130: 172-183.

Zhou, Y., Guan, W., Zhao, C., et al. Spontaneous imbibition behavior in porous media with various hydraulic fracture propagations: A pore-scale perspective. Advances in Geo-Energy Research, 2023, 9(3): 185-197.